Performance Evaluation of a Scaled-Up Membraneless Organic-Based Hybrid Flow Battery

Feilin Yu [1], Wenbo Zhao [1], Puiki Leung [1,*], Mohd Rusllim Mohamed [2], Lei Wei [3,*], Akeel Shah [1] and Qiang Liao [1]

1 Key Laboratory of Low-Grade Energy Utilization Technologies and Systems, MOE, Chongqing University, Chongqing 400030, China; feilinyu@cqu.edu.cn (F.Y.); wenbozhao@stu.cqu.edu.cn (W.Z.); akeelshah@cqu.edu.cn (A.S.); lqzx@cqu.eud.cn (Q.L.)

2 Faculty of Electrical and Electronics Engineering Technology, Universiti Malaysia Pahang, Pekan 26600, Malaysia; rusllim@ump.edu.my

3 Department of Mechanical and Energy Engineering, SUSTech Energy Institute for Carbon Neutrality, Southern University of Science and Technology, Shenzhen 518055, China

* Correspondence: p.leung@cqu.edu.cn (P.L.); weil@sustech.edu.cn (L.W.)

1. Model assumptions and development

The three-dimensional geometry of the battery model, encompassing free-flowing channels, positive and negative electrodes are illustrated in **Figure 1**. The porous carbon and metallic zinc electrodes were positioned on the right and left-hand side of the diagram, respectively. The thickness of the deposited metal zinc relative to the inter-electrode distance was considered negligible. The model assumed uniformity in the texture and viscosity of the electrode and electrolyte, as well as insulation and stable battery operation. Furthermore, the electrolyte was considered an incompressible fluid. The zinc chloride and hydroquinone (HQ) solutions were contained in an external storage tank and were delivered into the battery *via* an external pipeline using a pump in the charging process. In the present model, pipelines and pumps were excluded and substituted by Global Ordinary and Differential Equation (ODEs and DAEs) interfaces. During the charge processes, metallic zinc was electrodeposited on the negative electrode, while p-benzoquinone (BQ) was produced on the positive electrode. Conversely, during discharge, electrolyte flowed through the battery, and BQ was reduced to HQ on the positive electrode, while divalent Zn^{2+} ions formed on the negative electrode. The reaction equations for the typical charge-discharge cycling experiment are shown as follows:

At the negative electrode:

$$Zn^{2+} + 2e^{-} \leftrightharpoons Zn \tag{1}$$

At the positive electrode:

$$BQ + 2e^{-} + 2H^{+} \leftrightharpoons HQ \tag{2}$$

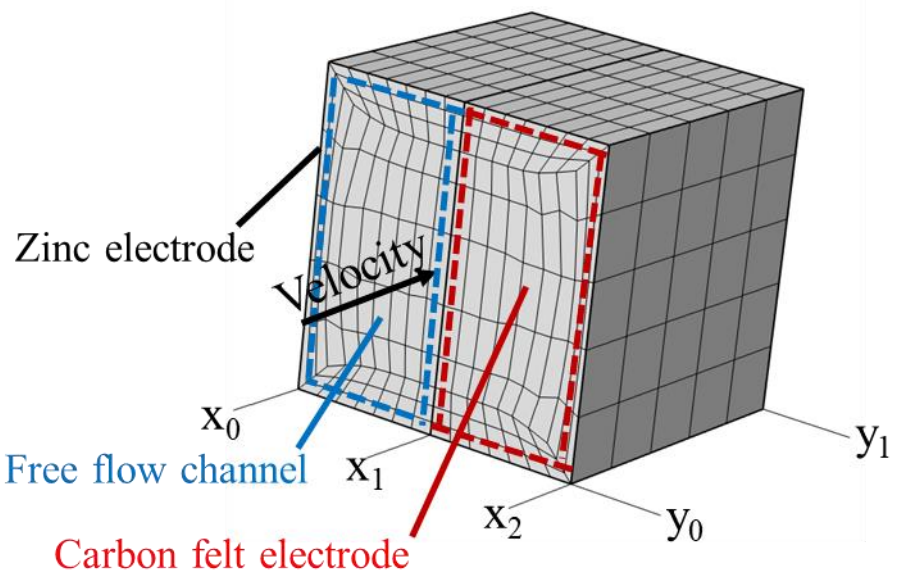

Figure S1. Schematic diagram of membraneless flow battery model

1.1 Mass transfer and fluid flow

The mathematical model was comprised of electrodes and electrolyte, whereby the electrolyte consisted of zinc chloride solution and hydroquinone solution, forming Cl^-, H^+, Zn^{2+}, BQ, and HQ during charging and discharging. These species were mass-conserved throughout the battery cycle, as derived from the Nernst-Planck equation in both the free channel and porous electrode.

$$\frac{\partial c_i}{\partial t} + \nabla \cdot \left(- D_i \nabla c_i - \frac{z_i c_i D_i}{RT} \mathrm{F} \nabla \phi + \boldsymbol{u} c_i \right) = 0 \tag{3}$$

$$\frac{\partial (\epsilon c_i)}{\partial t} + \nabla \cdot \left(- D_i^{eff} \nabla c_i - \frac{z_i c_i D_i^{eff}}{RT} \mathrm{F} \nabla \phi + \boldsymbol{u}_{eff} c_i \right) = S_i \tag{4}$$

Porosity was denoted by ε, whereas R, T, and F represented the molar gas constants, electrolyte temperature, and Faraday constants, respectively. The concentration, diffusion coefficient, valence state, and source term of species i were represented by c_i、D_i、z_i and S_i, whereas the ion potential, electrolyte flow rate, and effective electrolyte flow rate were denoted by ϕ、$\boldsymbol{u}$ and $\boldsymbol{u}_{eff}$, respectively. Within the porous electrode, the diffusion coefficient, D-i., underwent correction by Bruugeman, resulting in the effective diffusion coefficient D_i^{eff}:

$$D_i^{eff} = \epsilon^{3/2} D_i \tag{5}$$

The effective flow rate in a porous electrode was obtained by Brinkman's equation:

$$\nabla p = -\frac{\mu}{\kappa} \epsilon u_{eff} + \mu \nabla^2 u_{eff} \tag{6}$$

Here, the variables p, κ, and μ denoted the pressure, permeability coefficient, and dynamic viscosity, respectively. To determine the electrolyte flow rate $\boldsymbol{u}$ and pressure p, we employed the continuity equation and the Navier-Stokes equation for incompressible fluids, utilizing the dynamic viscosity and density of water.

$$\nabla \cdot u = 0 \tag{7}$$

$$\rho \frac{\partial \boldsymbol{u}}{\partial t} + \rho (u \cdot \nabla) \boldsymbol{u} = -\nabla p + \mu \nabla^2 \boldsymbol{u} \tag{8}$$

1.2 Conservation of charge electrochemical reactions

The electrolyte used in the battery was assumed to be electrically neutral, giving rise to the equation (9):

$$\sum_i z_i c_i = 0 \tag{9}$$

The conservation of charge applies, which states that the amount of charge $\boldsymbol{i}_l$ entering the electrolyte equals the amount of charge $\boldsymbol{i}_s$ leaving the solid electrode (equation 10).

$$\boldsymbol{\nabla} \cdot \boldsymbol{i}_l + \boldsymbol{\nabla} \cdot \boldsymbol{i}_s = 0 \tag{10}$$

The electrolyte current density is expressed as follows:

$$\boldsymbol{i}_l = -\sigma_l \nabla \phi - F \sum_i z_i D_i \nabla c_i \tag{11}$$

where σ_l. is the electrolyte conductivity, which can be obtained from equation 12.

$$\sigma_l = \frac{F^2}{RT} \sum_i z_i^2 D_i \nabla c_i \tag{12}$$

In the porous electrode, the conductivity was corrected by Bruugeman to obtain an effective conductivity σ_s^{eff}, as expressed in equation 13.

$$\sigma_s^{eff} = \epsilon^{3/2} \sigma_s \tag{13}$$

Moreover, the source term expression of the conservation of mass in the porous electrode can be obtained from the net current density, as shown in equation 14.

$$S_i = \frac{A v_i \boldsymbol{i}}{2F} \tag{14}$$

where, *A* represents the specific surface area of the porous electrode, and v_i is the stoichiometric coefficient of the chemical reaction of the species ***i***.

1.3 Electrochemical reactions

The electrochemical reactions taking place at the positive and negative electrodes could be described by the Butler-Volmer equation, expressed as equations (15) and (16), respectively.

$$\boldsymbol{i_{pos}} = AFk_{pos}\left(a_{HQ}\right)^{\alpha_{pos}}\left(a_{PQ}\right)^{1-\alpha_{pos}}\left[exp\left(\frac{(1-\alpha_{pos})nF\eta_{pos}}{RT}\right) - exp\left(-\frac{\alpha_{pos}F\eta_{pos}}{RT}\right)\right] \tag{15}$$

$$\boldsymbol{i_{neg}} = Fk_{neg}\left(a_{Zn(II)}\right)^{1-\alpha_{neg}}\left[exp\left(\frac{(1-\alpha_{neg})nF\eta_{neg}}{RT}\right) - exp\left(-\frac{\alpha_{neg}F\eta_{neg}}{RT}\right)\right] \tag{16}$$

The reaction rate constant in the positive and negative electrode was denoted by k_{pos} and k_{neg}, respectively. The activity of the species *i* (instead of concentration in this model) was represented by a_i, and *n* represented the number of electron transfers in the reaction. The charge transfer coefficients of the positive and negative electrode reaction were represented by α_{pos} and α_{neg}, respectively. The overpotential of the positive and negative electrodes was represented by η_{pos} and η_{neg}, respectively, as follow:

$$\eta = \phi_s - \phi_l - E_{eq} \tag{17}$$

The equilibrium potential E_{eq} of the reaction at both the positive and negative electrodes was given by the Nernst equation, expressed as equations (18) and (19):

$$E_{eq}^{pos} = E_0^{pos} + \frac{RT}{nF} ln\left(\frac{(c_{PQ})(c_H)^2}{c_{HQ}}\right) \tag{18}$$

$$E_{eq}^{neg} = E_0^{neg} + \frac{RT}{nF} lnc_{z_n(II)} \tag{19}$$

where E_0^{pos} and E_0^{neg} were the standard potentials of the positive and negative electrodes, respectively.

1.4 Boundary conditions

Transient studies are conducted in this model, with boundary conditions discussed

in **Figure 1**. At x_0 and x_2, matter transfer was zero at all external boundaries, while electron transfer was zero at y_0 and y_1. The boundary conditions were subject to the Neumann condition, except for the import and export, with the following expression:

$$\nabla p \cdot \boldsymbol{n} = \mathbf{0}\ (except\ inlets/outlets\ bonudary) \tag{20}$$

At the inlet, the electrolyte entered the battery at a certain flow rate and concentration under the action of the pump, and the boundary conditions were:

$$U = U_{in} \tag{21}$$

$$c = c_i^{in} \tag{22}$$

At the outlet, the diffusion flux was zero, and the pressure boundary conditions were as follows:

$$-D_i \nabla c_i \cdot \boldsymbol{n} = 0 \tag{23}$$

$$p = p_{out} \tag{24}$$

During the charge and discharge processes, the negative electrode was set to ground, and the positive voltage was hence the battery voltage. The pump recirculates the electrolyte by flowing from the reservoir through the pipe through the battery to store and release electricity, respectively. This process affected the electrolyte flow rate and concentration distribution and then affected the battery performance, which required attention. The volume flow Q at the outlet boundary was: $Q = U_{in}A_{out}$, where A_{out} was the outlet cross-sectional area. The average concentration at the outlet boundary was:

$$c_i^{out} = \int_{y=h} c_i dx \tag{25}$$

Assuming instantaneous mixing and ignoring the reaction in the reservoir, the conservation of mass was then obtained:

$$\frac{dc_i^{in}}{dt} = \frac{Q}{V_r}(c_i^{out} - c_i^{in}) \tag{26}$$

$$c_i^{in}(0) = c_i^0 \tag{27}$$

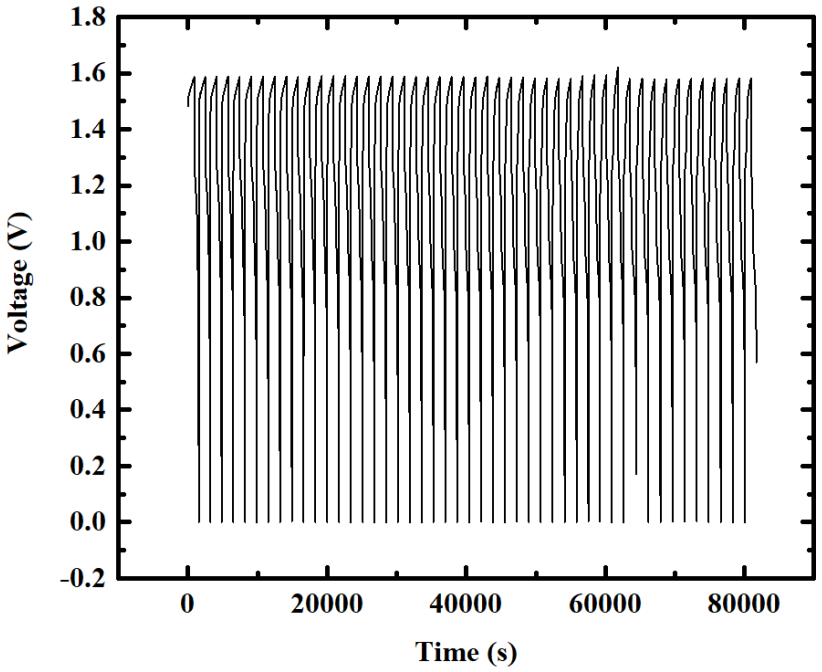

Figure S2. Test the 1 cm^2 electrode cell for 50 cycles at 10 mA cm^{-2} (charge and discharge for 15min, discharge cut-off voltage 0V)

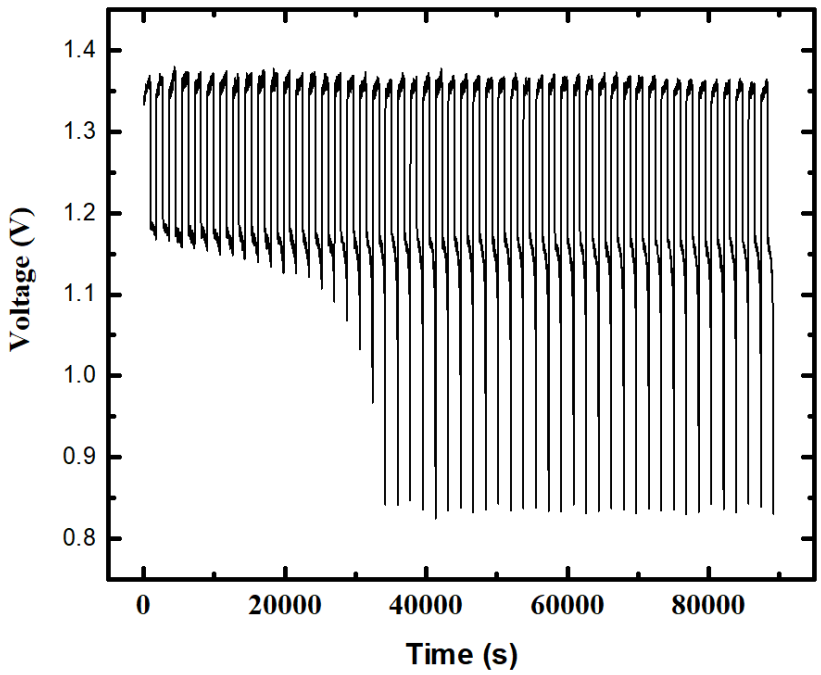

Figure S3. Test the 1600 cm^2 electrode cell for 50 cycles at 10 mA cm^{-2} (charge and discharge for 15min, cut-off discharge voltage 0V)

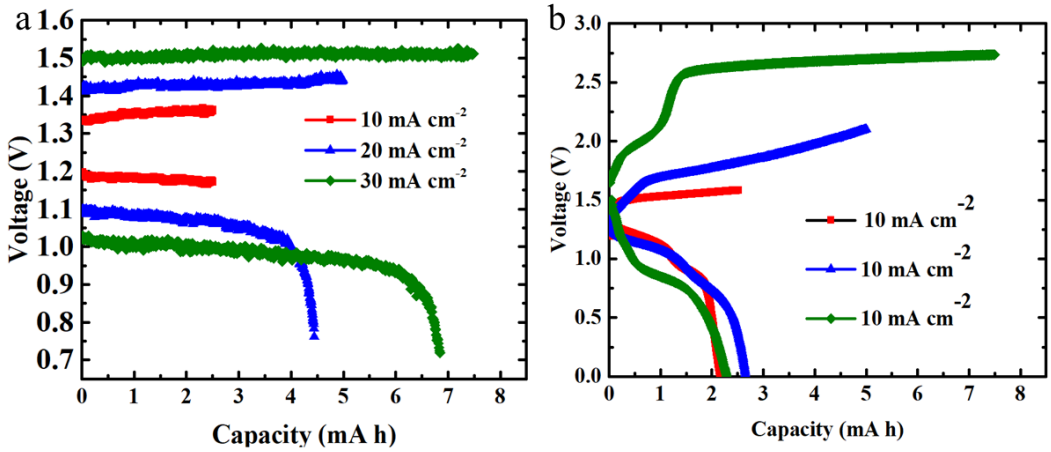

Figure S4. Capacity changes of (a)1600 cm^2 electrode cell and (b)1 cm^2 electrode cell during charging and discharging

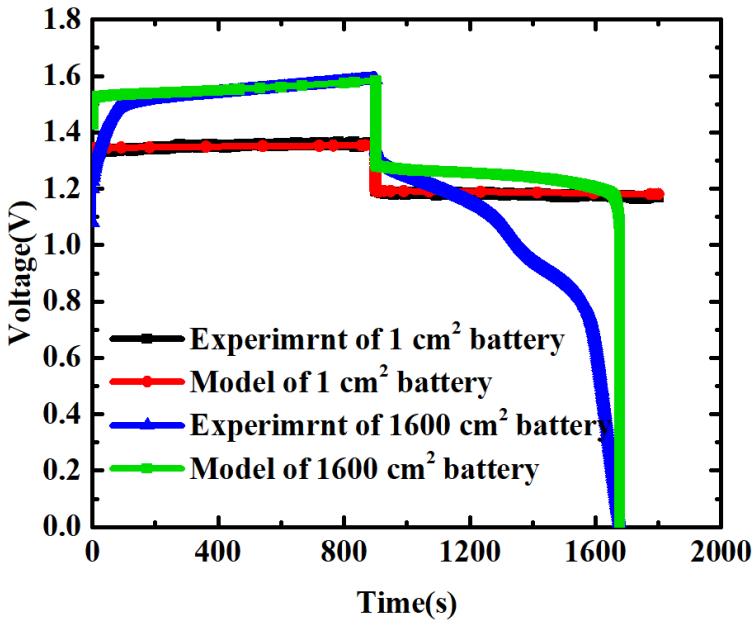

Figure S5. Comparison and validation of charging and discharging curves between model and experiment for 1 cm^2 and 1600 cm^2 electrode cell at 10 mA cm^{-2}.

There is good consistency between the experimental and model charging and discharging curves of 1 cm^2 electrode battery, indicating that the model can well reflect the facts.

During charging and discharging, 1600 cm^2 electrode battery generate sedimentary substance that covers the surface of carbon felt, which affects the performance of the battery. However, our model has been simplified without considering the impact of sediment on the battery (porosity, specific surface area, reaction rate), so there is a certain error on charge discharge curve between the experimental and the model.

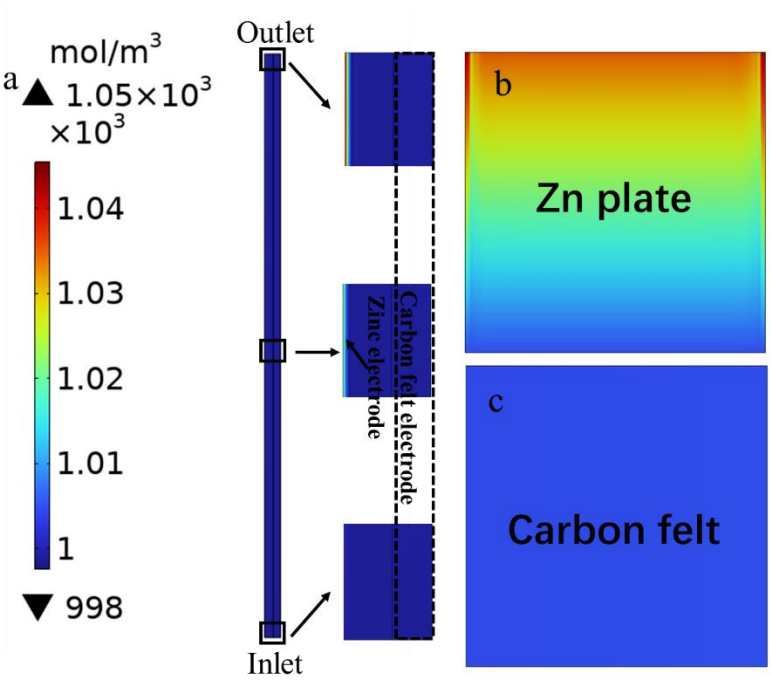

Figure S6. Distribution of the active zinc ion for a 1600 cm^2 electrode scaled-up battery at 10 mA cm^{-2} upon charging (at t = 1790s): The concentrations of zinc ion at the (b) cross-section; (c) negative electrode; (d) positive electrode.

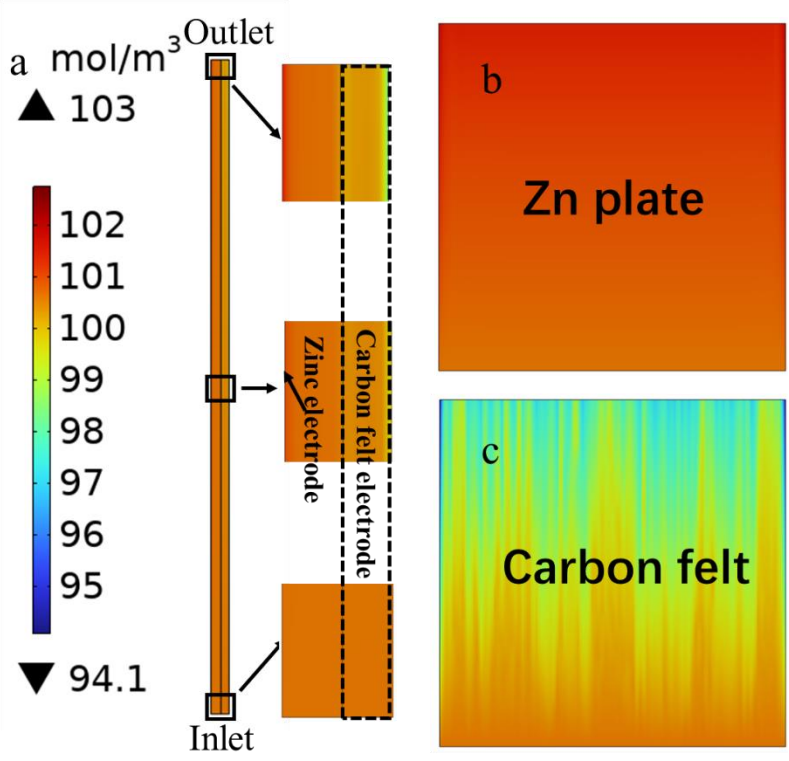

Figure S7. Distribution of the active p-benzoquinone species for a 1600 cm^2 electrode scaled-up battery at 10 mA cm^{-2} upon charging (at t = 1790s): The concentrations of zinc ion at the (b) cross-section; (c) negative electrode; (d) positive electrode.

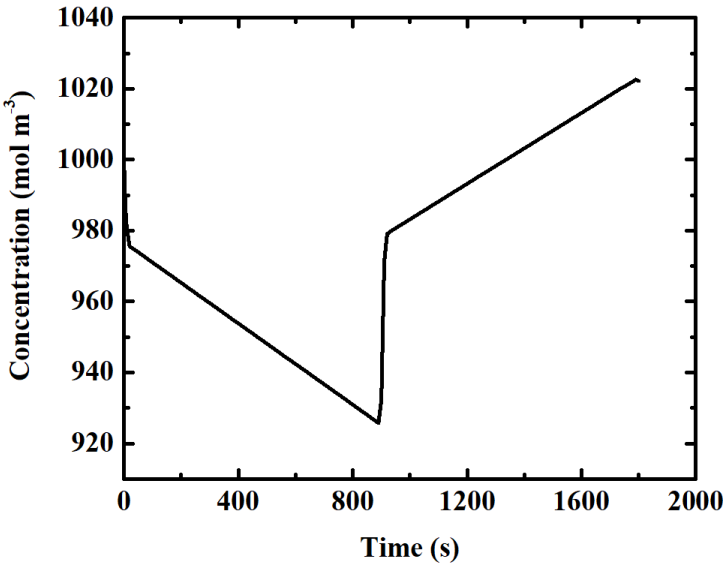

Figure S8. The variation curve of negative electrode zinc ion concentration with time.

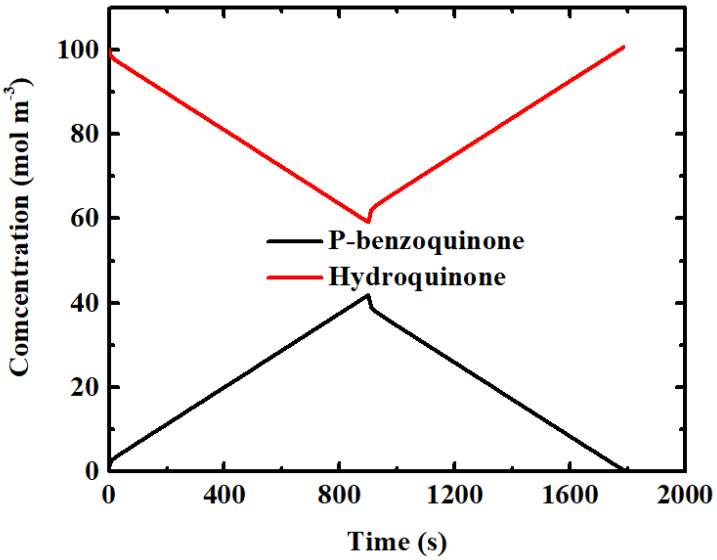

Figure S9. the variation curve of positive electrode hydroquinone and p-benzoquinone concentration with time.

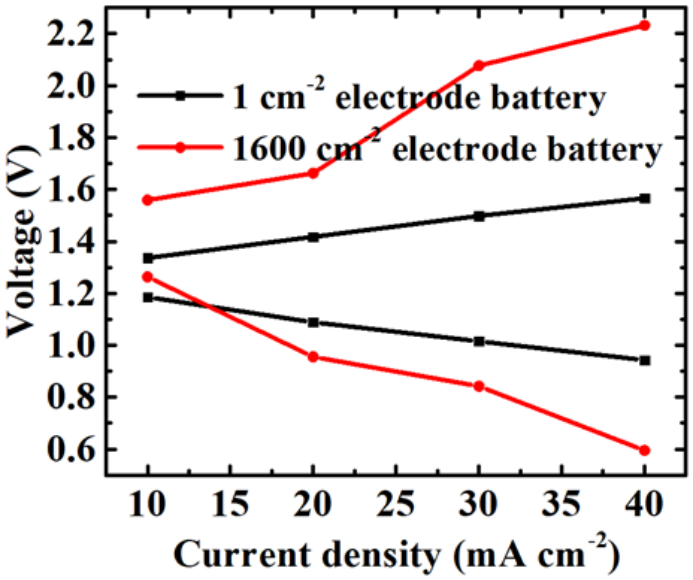

Figure S10. 1-minute voltage curve for charging/discharging of 1 cm^2 and 1600 cm^2 electrode battery at different current densities (10 - 40 mA cm^{-2}).

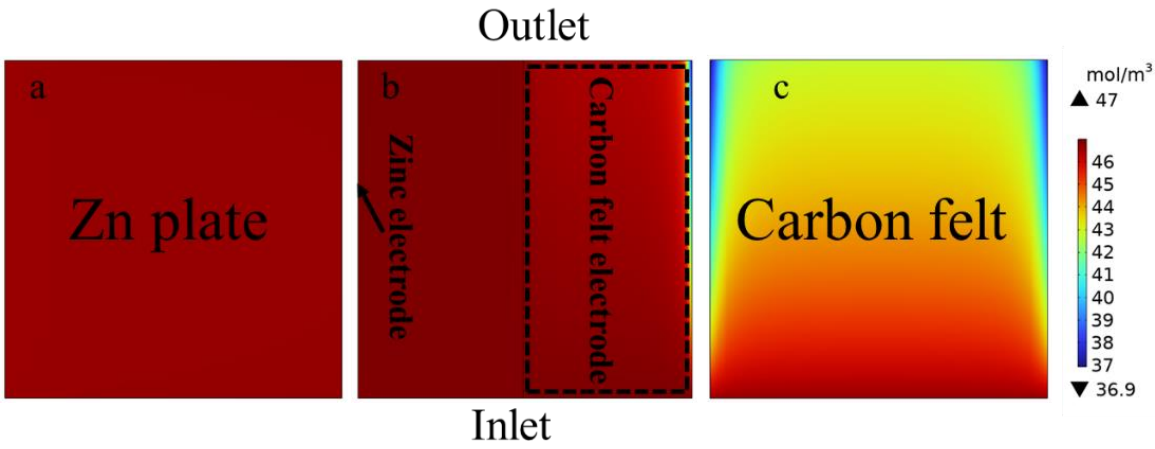

Figure S11. Distribution diagram of hydroquinone concentration for 1 cm^2 electrode battery at t=890s, I=10 mA cm^{-2}: (a) negative electrode; (b) cross-section; (d) positive electrode.

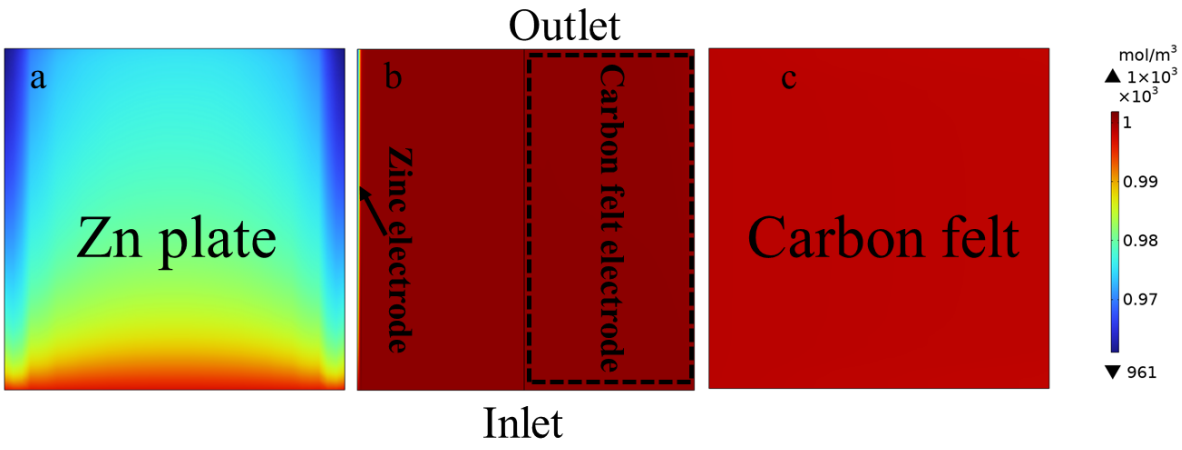

Figure S12. Distribution diagram of zinc ion concentration for 1 cm^2 electrode battery at t=890s, I=10 mA cm^{-2}: (a) negative electrode; (b) cross-section; (d) positive electrode.

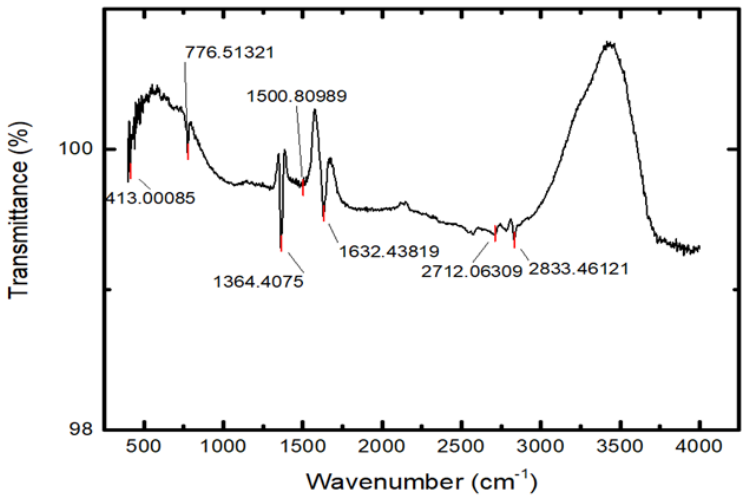

Figure S13. FTIR spectrum of the dried electrolyte suspension obtained from the experiment

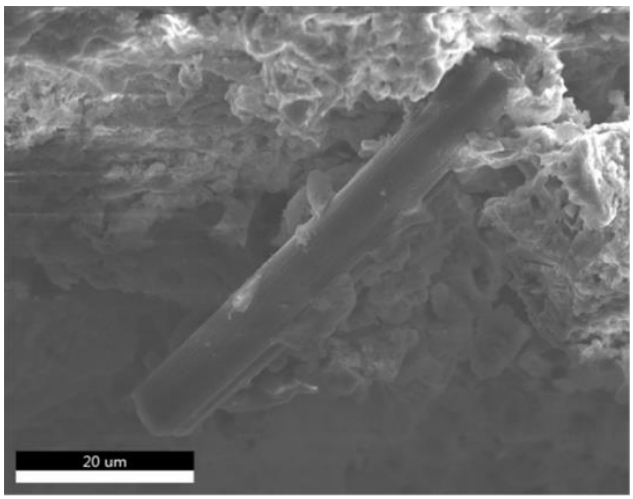

Figure S14. SEM image of the dried electrolyte suspension obtained from the experiment

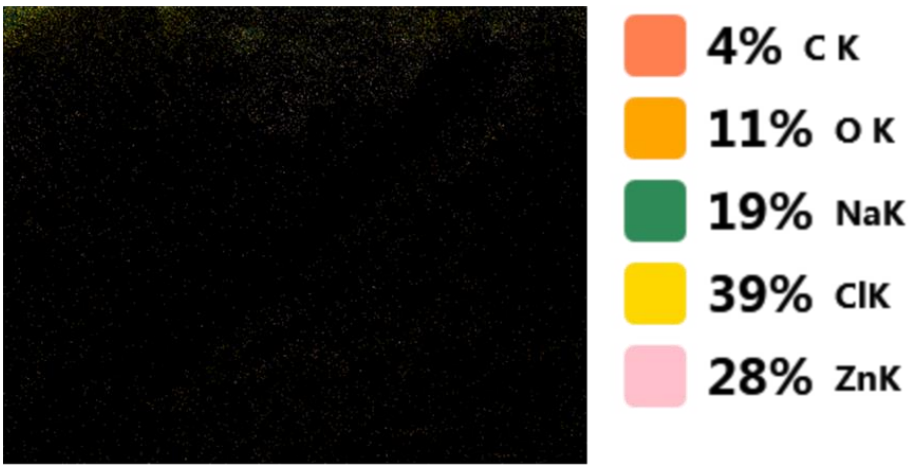

Figure S15. EDS Element distribution image of the dried electrolyte suspension obtained from the experiment

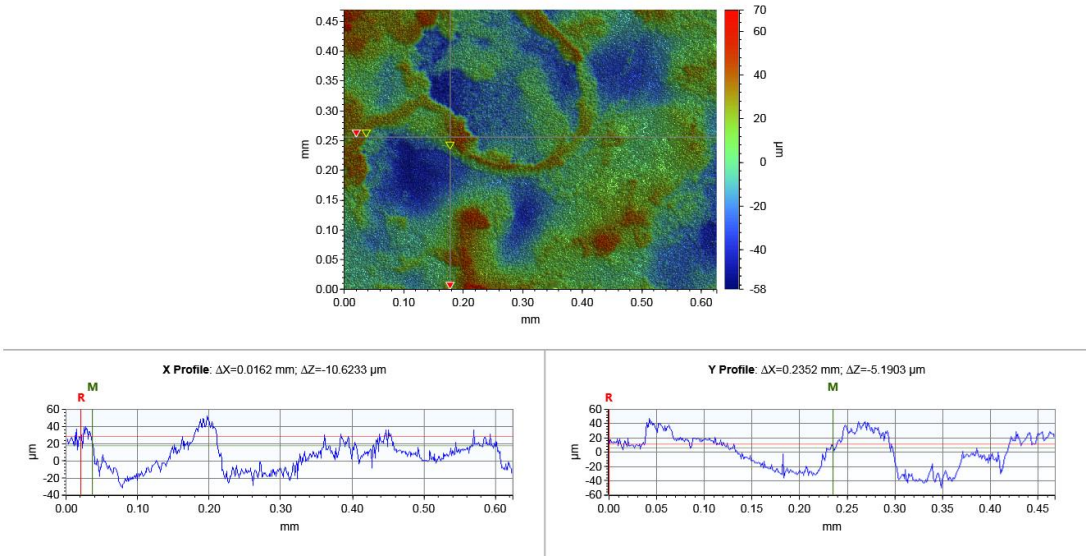

Figure S16. Three dimensions surface shape scanning results

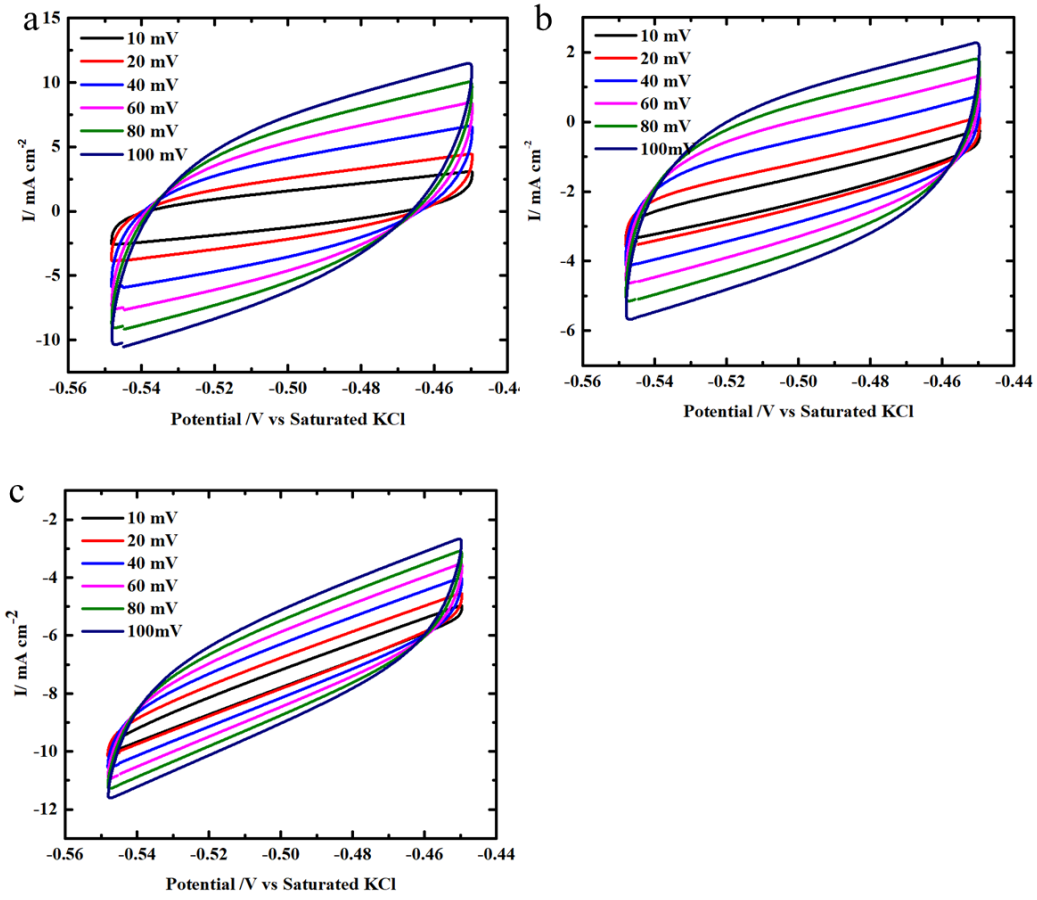

Figure S17. CV curves for (a) pristine carbon felt, carbon felt from (b) 1 cm^2 electrode battery and (c) 1600 cm^2 electrode battery in the region of -0.55 ~ -0.45 V vs. Saturated KCl with various scan rates.

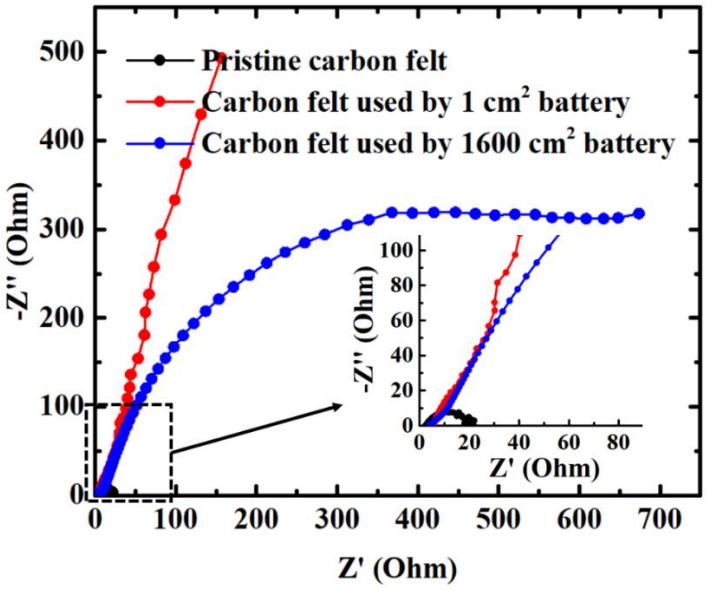

Figure S18 Nyquist plots of pristine carbon felt, carbon felt from 1 cm^2 electrode battery and 1600 cm^2 electrode battery.

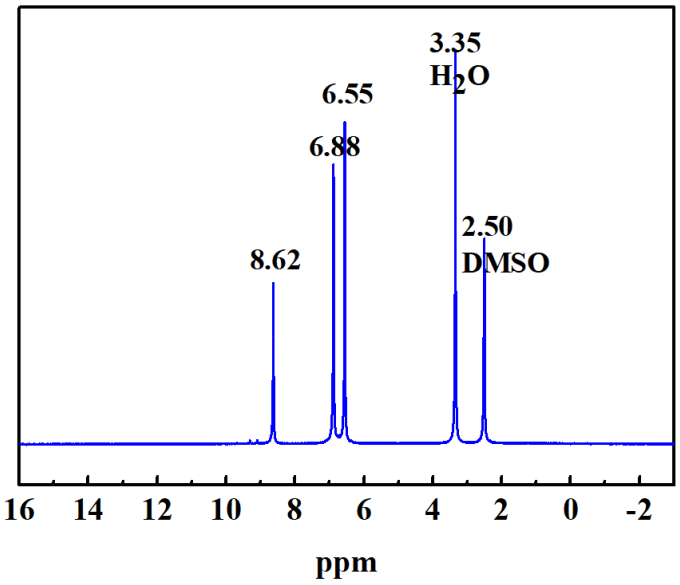

Figure S19. ^{1}H NMR of the solid substances collected on the positive carbon felt electrodes.

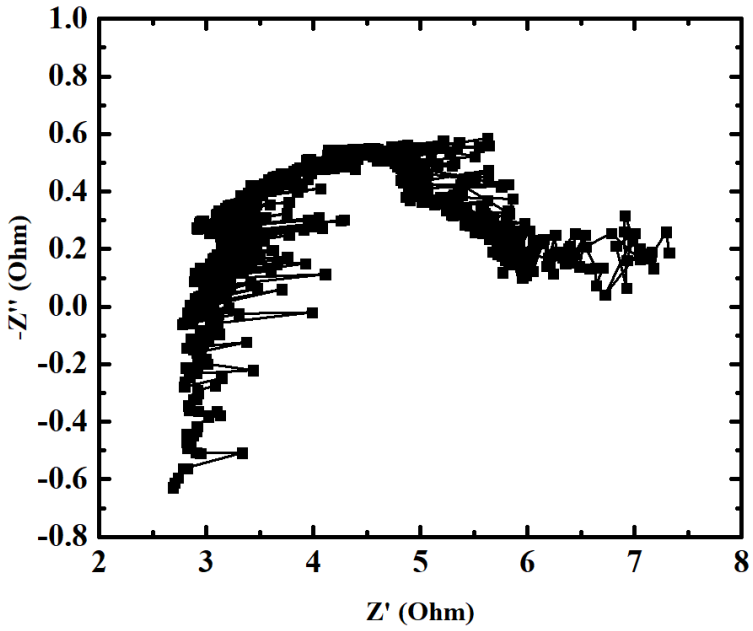

Figure S20. Nyquist plots of the 1 cm^2 electrode cell.

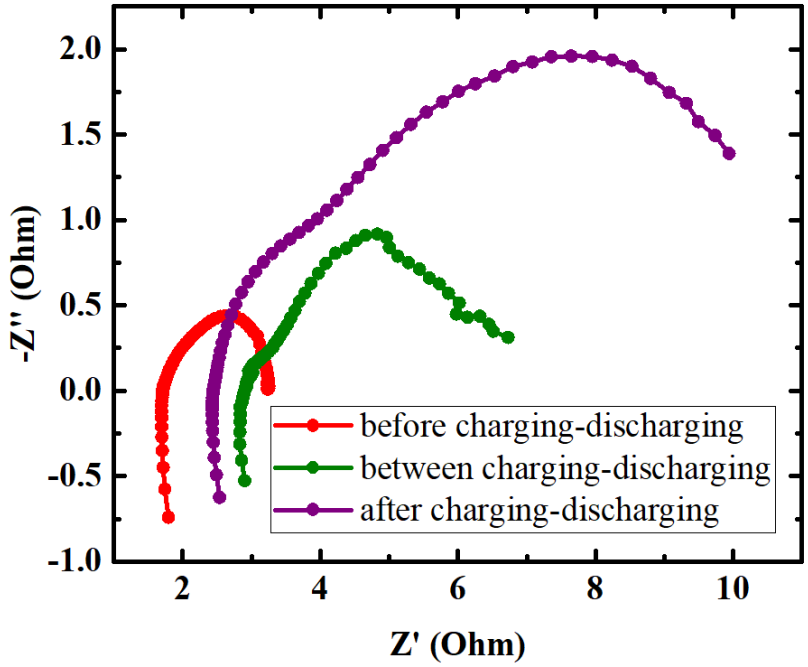

Figure S21. Nyquist plots of 1 cm^2 cell before/between/after charge-discharge cycles at 0% SOC.